Biosurface and Biotribology

WILEY

The Institution of Engineering and Technology

ORIGINAL RESEARCH OPEN ACCESS

Study of Pain From Skin Surface to Brain Responses Based on Mathematical Model

Yangyang Xia[1] | Yanze Wu[1] | Wei Tang[1] | Abdunabi Abduraufovich Kosimov[2] | Abdullo Mamadamon[2] | Shousheng Zhang[1] | Xingxing Fang[1]

[1]School of Mechanical and Electrical Engineering, China University of Mining and Technology, Xuzhou, Jiangsu, China | [2]Faculty of Digital Technologies, Systems, and Information Security, Tajik Technical University Named After Academician M.S. Osimi, Dushanbe, Tajikistan

Correspondence: Wei Tang (tangwei@cumt.edu.cn)

Received: 14 November 2025 | **Revised:** 20 January 2026 | **Accepted:** 23 January 2026

Keywords: γ oscillation | gate control theory | Hodgkin-Huxley model | pain | prosthetic liners

ABSTRACT

The excessive and continuous contacting pressure tends to cause skin injury and pain when the lower limb contacting with prosthetic liners. To relate the subcutaneous pressure and the brain response induced by pain sensations, a mathematical model was established based on the finite element model, Hodgkin–Huxley model and GCT model. The results showed that stronger subcutaneous pressure stimulation can lead to higher frequency of the membrane potential and T-cell potential. The frontal, prefrontal cortex, primary somatosensory cortex and occipital lobe were involved in the processing of pressure pain. A significant increase was observed in γ oscillations in pain states compared with no pain, but no significant differences in different pain level, indicating mathematical model and EEG methods can distinguish the pain but cannot distinguish the pain intensities when the stimulation exceeded the pain threshold. Compared with silicone materials, a higher T-cell potential and a lower pressure pain threshold were observed as the skin contacted with foam materials, suggesting that the foam materials can induce more severe pain on the skin surface. This study is helpful to understand the mechanisms of pain from skin surface to brain response and to provide theoretical guidance for the optimal design of lower limb prostheses.

1 | Introduction

Pain, as a physiological warning of the body's response to noxious stimuli, is an early sign of skin damage. Excessive or inappropriate stimuli of pressure causes sustained tissue deformation and cellular alterations, leading to pressure pain and even skin injury [1], such as pressure ulcers, induration and oedema [2–4]. The pressure pain is very common in the medical-related skin contact products, such as medical face mask, medical bed sheets and prosthesis [5–7]. Among them, the prosthetic is an essential way for the lower limb amputees to rebuild their walking ability. It is meaningful to investigate the mechanism of pressure pain for preventing and alleviating skin damage.

Nociceptive signals induced by the mechanical stimulation of the skin surface are conveyed to the primary and secondary somatosensory cortices of brain via the ascending pathways and generate the pain sensation after the comprehensive processing [8–10]. In previous studies, the endogenous analgesic system theory and central sensitivity theory were mainly focused on the local exchange of neurotransmitter related to pain sense [11, 12]. At present, the focus of research on the mechanism of pain transmission has been raised from the molecular and ion level to the whole nervous system [13, 14]. As the original region of pain transmission, human skin is a typical multilayered structure, mainly composed of epidermis, dermis and subcutaneous tissue. Nociceptors in the dermis may be activated and respond with depolarisation and action

potential generation when excessive pressure exerts onto the skin [15–17]. However, the stress and neurophysiological signals of the nociceptors in the dermis was difficult to measure. Finite element model (FEM) has been proved an efficient way to simulate the stress within the materials. In addition, previous studies have established many spike neuron models in order to clarify the generation of action potential, such as integrate-and-fire (IF) model [18], Hodgkin–Huxley (H–H) model [19] and Izhikevich model [20]. The action potential obtained from the neuron models transmits along primary afferents and provides input to the dorsal column in spinal cord, where preliminary screening and processing are performed [21]. In this field, the gate control theory (GCT) [22, 23] stated that a complex interneuron network in spinal cord modulates the transmission of sensory information from the primary afferent neurons to midbrain, acting as a 'gate'. When nociceptive information reaches a threshold that exceeds the inhibition elicited, it 'opens the gate' and activates pathways that lead to the pain sensation. The combination of neuron model and GCT has been proved to be able to simulate the transduction and modulation of action potential.

Brain is the centralised processing region for pain. Therefore, it is essential to understand the mechanisms of pain by studying the brain's response to pain. Electroencephalogram (EEG) has been widely used to study the brain activity related with sensation [24, 25]. Neural oscillations are the most prominent feature of EEG data, and previous studies have demonstrated that perceptual, cognitive, motor and emotional processes are highly related with specific patterns of oscillations [26, 27]. Among them, the gamma oscillations (30–100 Hz) play an important role in perceptual functions of brain, and the intensity of pain has been proved a strong association with the amplitude of gamma oscillations [28, 29].

In this study, the pressure contact between the prosthetic socket and the lower limb was taken as the research object. The generation and conduction mechanism of pressure pain from skin surface to neurophysiological brain responses was investigated, and a mathematical model was established combined with pressure pain threshold (PPT), FEM, H–H model and GCT model. This work contributes to understanding the triggered mechanism of pressure pain and provides theoretical support for the optimal design of lower limb prostheses.

2 | Experimental Details

2.1 | Samples

Based on the actual wearing of prosthesis, the load-bearing position of the lateral tibia (LT) was selected as skin anatomical region. Silicone and ethylene-vinyl acetate copolymer (EVA) foam, two commonly used prosthetic liner materials, were selected to press the skin anatomical region. A microcomputer control electronic universal testing machine (Hensgrand, Jinan, China) was used to measure the elastic modulus of the selected prosthetic materials. The elastic modulus and Poisson's ratio properties of prosthetic liner materials and typical anatomical region are shown in Table 1.

2.2 | Participants

Twenty healthy males aged 20–25 (mean ± standard deviation = 23.5 ± 2.1 years), participated in the study. All subjects were requested to provide written informed consent before the tests. This study was carried out according to international ethical standards and was approved by the Ethics Committee of Xuzhou Rehabilitation Hospital (No. XK-LSW-20240321-020).

This study has unified and limited the age and gender of the subjects. Although this recruitment criteria may limit the generalisability of this study, it can help reduce the influence of individual differences of the subjects on the results.

2.3 | Pain Threshold Evaluation

A numerical rating scale (NRS) was used in subjective evaluation to assess the pain sensation. The pain sensation is divided into four levels: no pain, mild pain, moderate pain and severe pain [30]. Specifically, a score of 0 indicates no pain, a score of 1–3 indicates mild pain, a score of 4–6 indicates moderate pain and a score of 7–10 indicates severe pain. The more intense the pain sensation, the higher the assessment score of pain sensation. According to references, the pressure pain threshold was measured using a designed pressure device as shown in Figure 1. A ball-on-flat mode was chosen to simulate the contact of the prosthetic socket/skin interface. The acrylic resin hemispherical indenters with diameter of 21 mm and covered with silicone and foam material were used, respectively.

During the test, a normal load was applied to the lower limbs, which is regulated by a sliding table and monitored by a triaxial force sensor. Corresponding to the NRS, the normal load was gradually increased from 5 N until the participant began to feel the mild pain and moderate pain, respectively. In the mild pain condition, the normal load is defined as the PPT. Since none of the subjects felt pain at the normal load of 10 N, 10 N was set as the normal load in the no pain condition.

2.4 | Reconstruction of Anatomic Regions Based on MRI Tomographic Images

MRI device (General Electric Medical System, Milwaukee, USA) was used to obtain the tomographic images of the lower limbs. The device was equipped with DICOM 3.0 international standard interface, and the images were output in DICOM standard format. The 3D Fiesta C sequence was selected to obtain accurate images of the dermis and epidermis. The scanning interval was 0.8 mm, the slice thickness was 0.4 mm, the plane resolution was 0.35 × 0.40 and the scan length was 60 mm (30 mm before and after the midpoint of the LT). Data collection began by performing two scout sequences, the first measuring 30 cm in width and the second 15 cm in order to focus the acquisition on the area to be explored and where the signal generated is the greatest.

The MRI tomographic images of the lower limbs were reconstructed in Mimics software (Materialise, Belgium) by recognising the grayscale values of the images and generate the point

cloud models for skin, subcutaneous tissue and muscles. In order to simplify the calculation process, the blood vessels and fibre structures of the lower limbs were ignored in the point cloud models. Then, the reconstructed point cloud models of LT were converted to shell models of curved surface in Geomagic software (Geomagic, USA) via overlaying and smoothing. Finally, the shell models were assembled with the models of the indenters in SOLIDWORKS software (Dassault Systemes, France) to complete the reconstruction of LT regions.

2.5 | Finite Element Modelling

To establish FEM, the reconstructed models were meshed with tetrahedral elements using HyperMesh software (Altair, USA). The elements were refined in the contact area with the indenter, with an element size of 1 mm in the dermis and epidermis, 2 mm in the subcutaneous tissues and 3 mm in the muscle tissues. The tetramesh method was applied to the 2-dimensional mesh to create 3-dimensional tetrahedral mesh. The total number of elements was 848, 344 for LT region. The material behaviour for different tissues in the model was simplified to be uniform isotropic linear elastomers, whereas the bones were assumed to be rigid elements and nondeformable. This simplification of viscoelastic properties of skin may result in a slight overestimation of maximum stress values as the actual stress relaxation in soft tissues cannot be simulated. The material constants of the LT regions and indenters were adapted as shown in Table 1.

TABLE 1 | Mechanical properties of prosthetic liner materials and typical anatomical region.

Material	Silicone liner	Foam liner covered with cotton socks	LT
Elastic modulus/MPa	0.1	0.94	0.06
Poisson's ratio	0.48	0.39	0.49

All nodes of the interface between muscle and bone were fixed in the LT region, resulting in nonconstricted boundary conditions. The indenter was fixed in two directions and allowed to move in the direction orthogonal to the skin surface. A contact surface between the tip of the indenter and the skin was defined, and the contact penalty factor was set constant. All calculations were carried out in ABAQUS software (Abaqus Inc, USA).

2.6 | EEG Test and Data Processing

A 32-channel acquisition system (ANT Neuro, Hengelo, Netherlands) was used to monitor the EEG signals related with the pressure pain of subject. Based on the results of the subjective evaluation, the subjects were stimulated under three pain sensation conditions (no pain, mild pain and moderate pain). The test procedure and location distribution of electrodes are shown in Figure 2. Firstly, EEG signals under resting state were recorded for 180 s as the baseline. Then, the skin of LT region was pressed by the silicone indenter for 30 s, immediately followed by 180 s of rest. The pressure stimulation was repeated 5 times under each pain conditions. All tests were conducted in a laboratory environment at a temperature of 26°C to 28°C and a relative humidity of 45%–65%.

The obtained EEG data were firstly bandpass filtered between 0.5 and 30 Hz and baseline corrected. Then, the five EEG data

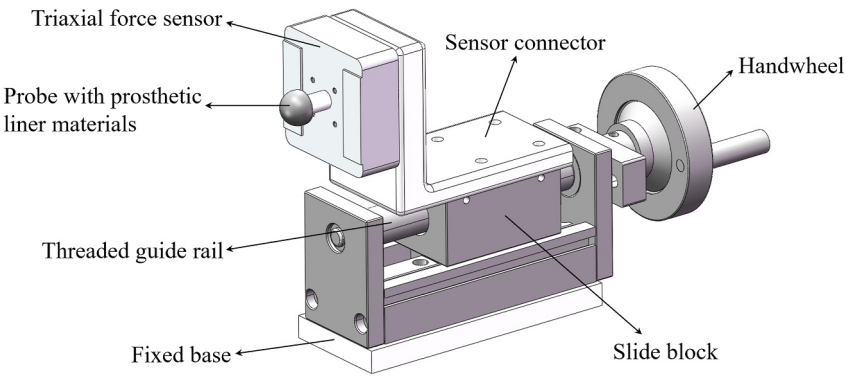

FIGURE 1 | Structure schematic diagram of test machine.

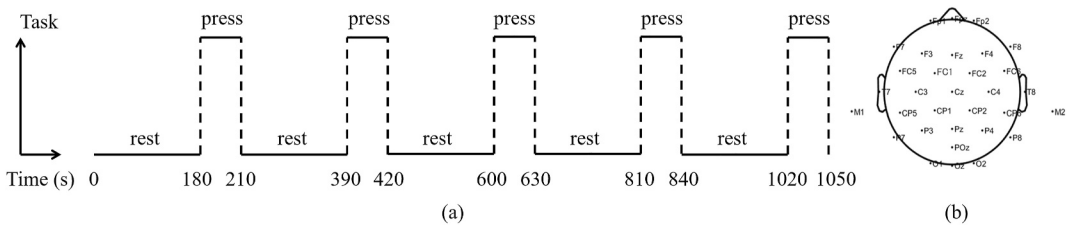

FIGURE 2 | (a) Test procedure of EEG recording and (b) location distribution of electrodes.

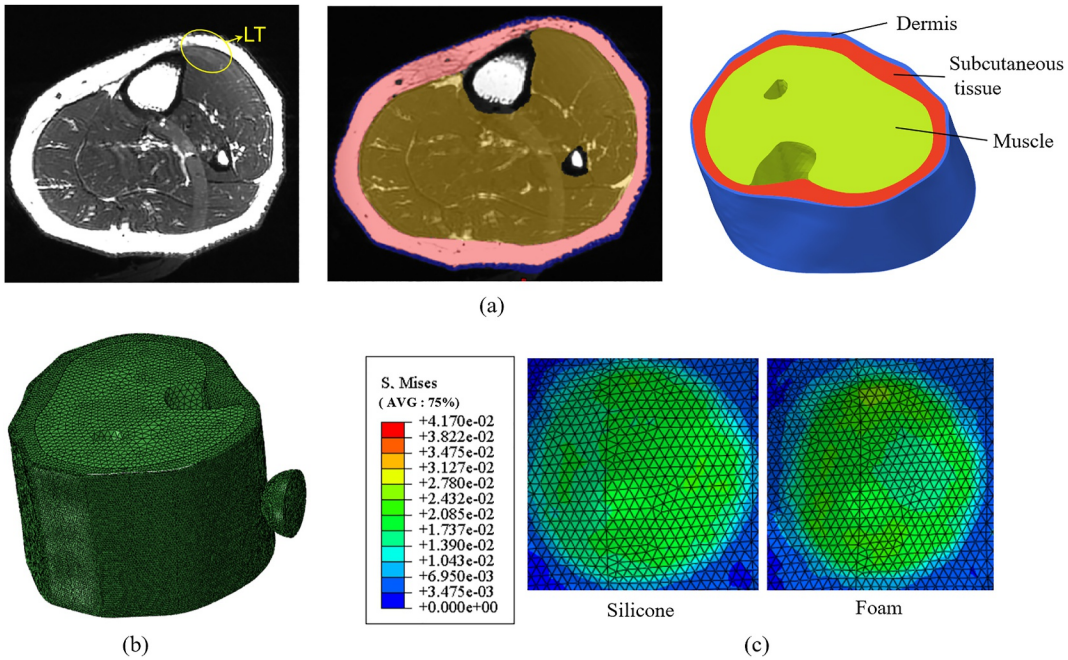

FIGURE 3 | (a) 3D reconstruction and (b) FEM of the LT region; (c) FEM simulated surface stress of the LT region under silicone and foam conditions.

segments were overlaid and averaged and transformed into the frequency domain using discrete Fourier transform method, obtaining a power spectrum of 1–100 Hz. To improve the signal-to-noise ratio, the obtained single channel power spectrum was averaged in each channel for each electrode. The amplitude of EEG oscillations for each electrode in the γ (30–100 Hz) band was calculated, and the power spectrum after baseline correction is normalised under different conditions in each frequency band and represented as the Z-value. All processing was carried out in MATLAB (Mathworks, USA).

3 | Results and Discussions

3.1 | FEM Simulation

The processing of 3D reconstruction and FEM of LT was shown in Figure 3a–b. To verify the accuracy of the FEM, the surface stress of the skin obtained from the test was compared with that from the FEM simulation under a normal load of 10 N condition. The tested surface stress of skin was calculated from the normal pressure and the contact area. The simulated surface stress of LT under silicone and foam conditions was determined by the average stress of the nodes in the compression area of the FEM as shown in Figure 3c. The comparison of the surface stress under the four contact interfaces conditions was shown in Table 2. The results showed that the result of FEM simulation was close to test stress, indicating the FEM can be used to simulate the stress distribution of the skin under pressure pain conditions.

According to the subjective evaluation, for the LT-silicone interface, the normal loads corresponding to three pain states (no pain, mild pain and moderate pain) were measured to be 10 N, 26.17 N and 37.13 N, respectively. The normal loads were applied to the FEM to obtain the maximum stress in the dermis. The maximum stress corresponding to the three pain states was 19.91 kPa, 38.49 kPa and 53.61 kPa, respectively as shown in Figure 4. The results showed that with the increase of the normal loads, the maximum stress in the dermis and the transmission depth of the stress also increased, indicating the nociceptors in the dermis were subjected to the stronger stimulation.

TABLE 2 | The surface stress of LT under silicone and foam conditions obtained from experiment and FEM simulation.

	LT-silicone	LT-foam
Experimental surface stress/kPa	17.47	14.15
FEM simulated surface stress/kPa	22.74	19.09

3.2 | Transduction, Modulation and Perception Models of Pressure Pain

The maximum stress (19.91 kPa, 38.49 kPa and 53.61 kPa) corresponding to the three pain states obtained from the FEM was input to the transduction model to generate neural impulses. When the nociceptors in the skin are mechanically stimulated, sodium ions (Na^+) and potassium ions (K^+) in the cells undergo osmotic exchange inside and outside the cell membrane, leading to changes in cell membrane potential V_m. Membrane potential is a key indicator of the degree of neural impulse and can be described using the H–H model. According to the theory of the classical H–H model, the total current of the cell membrane consists of the ions transportation and the current that charges the membrane capacity. For the modified H–H model, a fast transients current was added in the ion transportation part, which improved the sensitivity for changes in

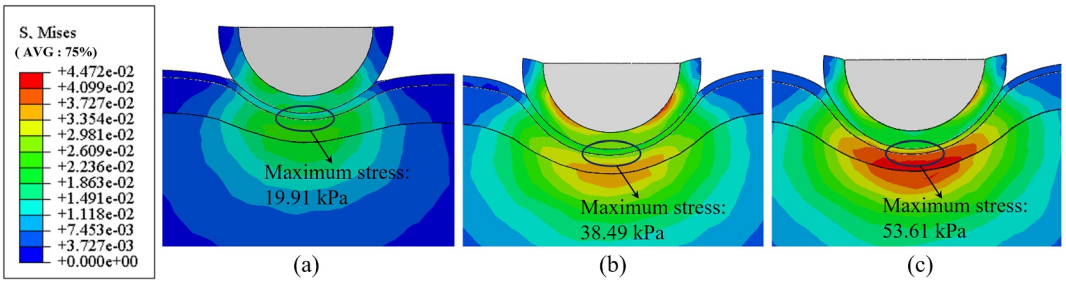

FIGURE 4 | Stress distribution inside the skin at (a) no pain, (b) mild pain and (c) moderate pain condition.

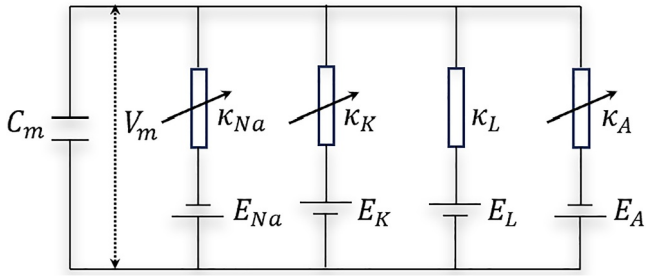

FIGURE 5 | Equivalent circuit of the H–H model.

membrane potential. This process can be simulated by establishing an equivalent circuit as shown in Figure 5.

The mathematical expression of the H–H model is as follows:

The total current of the cell membrane includes the parts of the transportation of ions and the current that charges the membrane capacity:

$$C_m \frac{dV_m}{dt} = I_{mech} + I_{shift} - (I_{Na} + I_K + I_A + I_L). \quad (1)$$

$$I_{mech} = \left[C_{m1} \exp\left(\frac{(\sigma - \sigma_t)/\sigma_t}{C_{m2}} \right) + C_{m3} \right] \times H(\sigma - \sigma_t). \quad (2)$$

V_m and t represent the membrane potential of the nociceptor and time, respectively. The frequency of V_m represents the intensity of mechanical stimulation, and C_m is membrane capacitance per unit area. I_{Na}, I_K, I_A and I_L correspond to the currents generated by sodium ions, potassium ions, fast transients and leakage current components, respectively. I_{shift} is the current to guarantee the action potential when $\sigma > \sigma_t$, and I_{mech} is an electrical current caused by mechanical stimulation. σ_t is the pressure pain threshold obtained from subjective evaluation results, and $H(x)$ is the Heaviside function. C_{m1}, C_{m2} and C_{m3} are constants related to mechanical stimuli. These three parameters are empirical constants optimised for specific cell types [31].

The ionic current I_{Na}, I_K, I_A and I_L driven by the membrane potential could be described as follows:

$$I_{Na} = g_{Na} m^3 h (V_m - E_{Na}), \quad (3)$$

$$I_K = g_K n^4 h (V_m - E_K), \quad (4)$$

$$I_A = g_A A^3 B (V_m - E_A), \quad (5)$$

$$I_L = g_L (V_m - E_L), \quad (6)$$

where E_{Na}, E_K, E_A and E_L are the reversal potentials as demonstrated in Figure 6. κ_i represents different ionic conductance here. The m, n, h, A and B are the gating variables satisfy:

$$\tau_x \frac{dx}{dt} + x = x_\infty, \quad (7)$$

where x represents the gating variables. For $x = m$, h and n, the expressions of τ_x and x_∞ are given as follows:

$$x_\infty = \frac{\alpha_x}{\alpha_x + \beta_x}, \tau_x = \frac{1}{\alpha_x + \beta_x}. \quad (8)$$

$$\alpha_m = \frac{(V_m + 29.7)/10}{1 - \exp(-(V_m + 29.7)/10)}, \quad \beta_m = 4 \exp(-(V_m + 54.7)/18). \quad (9)$$

$$\alpha_h = 0.07 \exp(-(V_m + 48)/20), \beta_h = \frac{1}{1 + \exp(-(V_m + 18)/10)}. \quad (10)$$

$$\alpha_n = \frac{(V_m + 45.7)/100}{1 - \exp(-(V_m + 45.7)/10)}, \quad \beta_n = 0.125 \exp(-(V_m + 55.7)/80). \quad (11)$$

For $x = A$ and B, the expressions for τ_x and x_∞ are follows:

$$\tau_A = 0.3632 + \frac{1.158}{1 + exp(V_m + 55.96)/20.12}, \quad A_\infty = 0.0761 \times \left(\frac{\exp(V_m + 94.22)/31.84}{1 + exp((V_m + 1.17)/28.93)} \right)^{1/3}, \quad (12)$$

$$\tau_B = 1.24 + \frac{2.678}{1 + \exp((V_m + 50)/16.027)}, \quad B_\infty = \left(\frac{1}{1 + \exp((V_m + 53.3)/14.54)} \right)^4, \quad (13)$$

V_m can be solved by substituting Equations (2–13) into Equation (1). Based on the modified H–H model, a nonlinear differential equation is used to simulate the electrical signal of neural impulses and a set of periodic membrane potential V_m curves are obtained as shown in Figure 7. The results indicated that the membrane potential curve showed a nonperiodic change state under no pain state, and when the mechanical stimulation exceeded the pressure pain threshold, the membrane potential

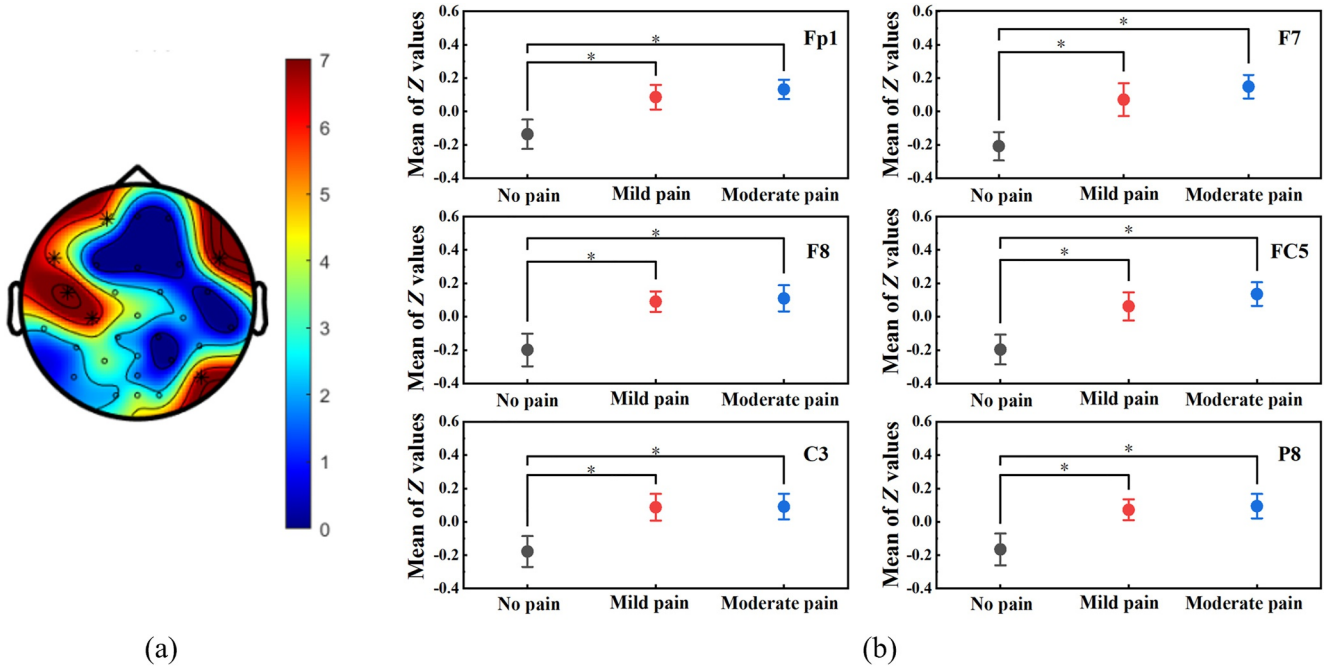

FIGURE 6 | (a) Scalp topography of normalised amplitude spectra of γ oscillations under three pain conditions and (b) mean values of Z values in the γ band under three pain states, asterisk * indicated pain states with a significant difference ($p < 0.05$).

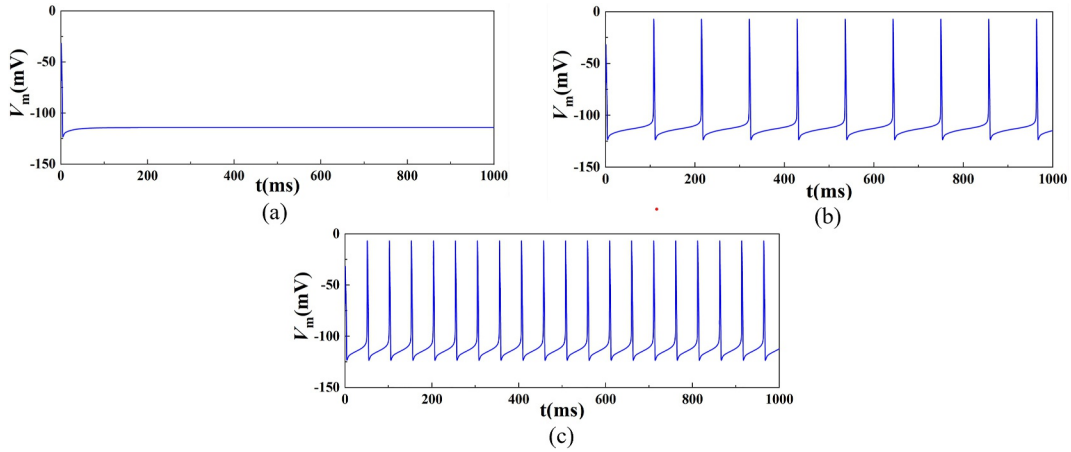

FIGURE 7 | Membrane potential variation at different pain conditions (a) no pain, (b) mild pain and (c) moderate pain.

frequency increased with the increasing of the pain state. According to previous studies, the frequency of the curve represented the strength of neural impulses. Under no pain state, the nociceptors were not activated, and there were no noxious neural signals. When the mechanical stimulation exceeded the pressure pain threshold, the exchange of ions was enhanced, which caused stronger noxious neural signals.

The frequency of membrane potential under three pain states obtained from the H-H model was transmitted to the GCT model. The GCT model can be used to describe the process of modulating and perceiving pain at the spinal dorsal horn, and the mathematical description is as follows:

$$0.7\frac{dV_i}{d_t} = -(V_i + 70) + 60\tanh(\theta_{li}x_l) + 40\tanh\big(f_b(V_b)\big), \quad (14)$$

$$0.7\frac{dV_e}{d_t} = -(V_e + 70) + 40\tanh(\theta_{se}x_s)\big[1 + 3\tanh\big(4f_e(V_e)\big)\big], \quad (15)$$

$$0.7\frac{dV_t}{d_t} = -(V_t + 70) + 40\tanh((1-\theta_{se})x_s) + 40\tanh((1-\theta_{li})x_l) + 40\tanh\big(f_e(V_e)\big) - 40\tanh\big(f_i(V_i)\big) - 40\tanh\big(f_b(V_b)\big), \quad (16)$$

$$0.7\frac{dV_b}{dt} = -(V_b + 70) + 40\tanh\big(f_t(V_t)\big), \quad (17)$$

V_i and V_e are the potentials of inhibitory substantia gelatinosa (SG) and excitatory substantia gelatinosa, and V_t is the potential of central T-cell present in the spinal dorsal horn. The subscripts l and s represent large nerve fibres and small nerve fibres,

respectively. Substituting the fluctuation frequency of membrane potential at x_l, the function of $f_j(V_j)$ can be expressed as follows:

$$f_j(V_j) = \left(\frac{V_j - V_{\text{thr}}}{-V_{j0}}\right) \times H(V_j - V_{\text{thr}}), \tag{18}$$

where the subscript j represents i, e, t and b in the equation. $V_{j0} = -70$ mV is the initial membrane potential.

Figure 8 showed the variation of T-cell potentials at different pain states. According to previous study, V_t reflects the strength of neural potential transmitted to the thalamus and directly affects the intensity of stimulation received by the cerebral cortex. The results of T-cell potentials showed that under the no pain state, V_t presents a horizontal straight line, indicating that no noxious neural electrical signals are transmitted to the brain. When the stress was detected to exceed the PPT, V_t showed an upward trend with the increase of stress, indicating that the noxious neural signals transmitted to the brain are becoming stronger, resulting in stronger pain sensation in the cerebral cortex.

3.3 | EEG Analysis

The T-cell potential formed after modulation by the dorsal horn of the spinal cord was conducted upwards through the thalamus and ultimately generates pain in the cerebral cortex. In order to study the neurophysiological responses of the brain under the three pain states and reveal the complete process of pressure pain, EEG signals were detected in the experiment. Figure 6 (a) showed the scalp topography of normalised amplitude spectra of γ oscillations under three pain states. The results suggested that significant difference in γ band (30–100 Hz) was found in prefrontal cortex (PFC), frontal cortex (FC), primary somatosensory cortex (SI) and occipital lobe (OL) under three pain states, and the corresponding electrodes were Fp1, F7, F8, FC5, C3 and P8. Furthermore, to determine the significant differences between the different states, Figure 6 (b) showed the mean values of Z values in the γ band for the mentioned electrodes. The least significant difference (LSD) tests suggested that compared with no pain states, the mean values of Z values in the γ band were significantly ($p < 0.05$) enhanced under painful states. However, no significant difference ($p > 0.05$) was found between the mild pain and moderate pain states.

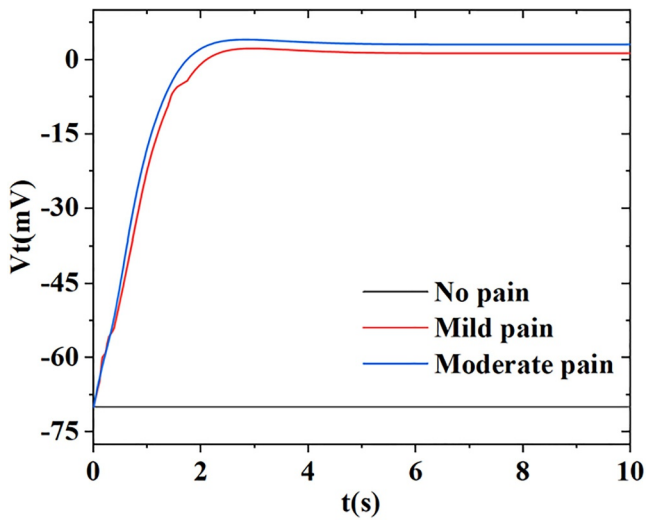

FIGURE 8 | Variation of T-cell potentials at different pain conditions.

According to previous research, the γ oscillation represents the summary effects of bottom–up stimulus-related and top–down subject-driven cognitive processes, which constituted the mechanism for integrating low-level cortical processing of basic stimulus features and high-level cognitive processes (e.g., attention and anticipation). Enhanced γ oscillation showed that more attention was activated. Compared with no pain state, painful stimulation led to higher T-cell potentials, which ultimately form different levels of pain evaluation through subject driven cognitive integration in the cerebral cortex, and are reflected by γ oscillation intensity. However, the difference of brain response between the mild pain state and moderate pain state cannot be recognised by the EEG method. Combined with the simulation results of GCT, the difference of T-cell potential between mild pain and moderate pain states is only about 2 mV, which indicated that after the integrating of cognition processes, the subtle difference in T-cell potential was unified.

3.4 | Influence of the Prosthetic Liner Materials on Pain Sensation

Based on the obtained H–H and GCT models, the influence of the prosthetic liner materials on pain sensation was carried out. According to the subjective evaluation, the PPT of the LT region under silicone and foam was 26.17 and 19.64 N, respectively, which suggested that foam materials are more likely to cause discomfort.

To verify the mathematical model of pressure pain, a normal load of 23 N between the PPT interval of silicone and foam materials was chosen to apply in the FEM. According to the FEM model, the maximum subcutaneous stress was 34.36 and 35.14 kPa when contact with silicone and foam. The maximum stress obtained from the FEM was input to the H–H model to simulate the membrane potential of LT regions. The results showed a constant wave of the membrane potential under foam material conditions, whereas the membrane potential under silicone material conditions was shown in baseline as shown in Figure 9a–b. Furthermore, the frequencies obtained from the membrane potential curves were input to the GCT model to obtain the T-cell potential, and the results are shown in Figure 9c. The T-cell potential presents a straight line under silicone conditions, indicating that no noxious neural electrical signals are transmitted to the brain. Under foam material conditions, the T-cell potential showed an upward trend, indicating that the noxious neural signals transmitted to the brain, resulting in pain sensation in the cerebral cortex. The simulation results corresponded to the results of the subjective evaluation, namely, a normal load of 23 N did not induce the pain sensation for silicon, and induce the pain sensation for foam.

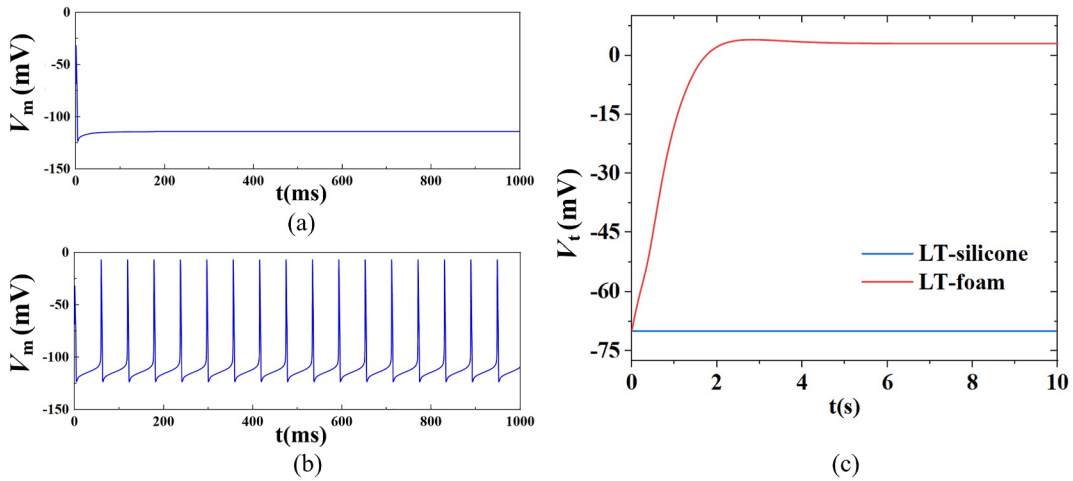

FIGURE 9 | Membrane potential variation of LT under (a) silicone, (b) foam materials and (c) the variation of T-cell output from the LT regions.

4 | Conclusion

The transmission mechanism of pressure pain was systematically investigated from skin surface to brain responses based on mathematical model including FEM, H-H model, GCT model and EEG methods. The main conclusions are as follows.

1. H-H model and GCT model can be used to build pain conduction pathway, which can connect the subcutaneous pressure and the brain response induce by pain. Stronger subcutaneous pressure stimulation can lead to higher frequency of the membrane potential of H–H model and T-cell potential of GCT model, indicating that more noxious information was transmitted in the spinal cord. Hence, an enhancement in γ oscillations of EEG was evoked by increased pressure pain within the FC, PFC, SI and OL.
2. Significant differences were found in γ oscillations and T-cell activity between no pain and painful states; however, no significant differences between mild pain and moderate pain, indicating that the mathematical model and EEG methods can distinguish the pain, but cannot distinguish the pain intensities when the stimulation exceeded the pain threshold.
3. When skin contacted with foam liner materials, a higher T-cell potential and a lower PPT were observed, suggesting that the foam materials can induce more severe pain on the skin surface compared with silicon liner.

Acknowledgements

The authors acknowledge financial support from the National Natural Science Foundation of China (Grant 52375224) and Natural Science Foundation of Jiangsu Province (Grant BK20242086).

Conflicts of Interest

The authors declare no conflicts of interest.

Data Availability Statement

The data that support the findings of this study are available from the corresponding author upon reasonable request.

References

1. A. Gefen and E. Soppi, "What Is New in Our Understanding of Pressure Injuries: The Inextricable Association Between Sustained Tissue Deformations and Pain and the Role of the Support Surface," *Wound Practice & Research: Journal of the Australian Wound Management Association* 28, no. 2 (2020): 58–65, https://doi.org/10.33235/wpr.28.2.58-65.

2. S. Gershon, "Using Subepidermal Moisture Level as an Indicator of Early Pressure Damage to Local Skin and Tissue," *Advances in Skin & Wound Care* 33, no. 9 (2020): 469–475, https://doi.org/10.1097/01.asw.0000655380.86380.7b.

3. A. Gefen and K. Ousey, "Update to Device-Related Pressure Ulcers: SECURE Prevention. COVID-19, Face Masks and Skin Damage," *Journal of Wound Care* 29, no. 5 (2020): 245–259, https://doi.org/10.12968/jowc.2020.29.5.245.

4. D. Jackson, L. Durrant, E. Bishop, et al., "Pain Associated With Pressure Injury: A Qualitative Study of Community-Based, Home-Dwelling Individuals," *Journal of Advanced Nursing* 73, no. 12 (2017): 3061–3069, https://doi.org/10.1111/jan.13370.

5. B. Hajhosseini, M. T. Longaker, and G. C. Gurtner, "Pressure Injury," *Annals of Surgery* 271, no. 4 (2020): 671–679, https://doi.org/10.1097/sla.0000000000003567.

6. S. G. da S. Galetto, E. R. P. d. Nascimento, P. M. V. Hermida, and L. B. H. d. Malfussi, "Medical Device-Related Pressure Injuries: An Integrative Literature Review," *Revista Brasileira de Enfermagem* 72, no. 2 (2019): 505–512, https://doi.org/10.1590/0034-7167-2018-0530.

7. S. A. Kayser, C. A. VanGilder, E. A. Ayello, and C. Lachenbruch, "Prevalence and Analysis of Medical Device-Related Pressure Injuries: Results From the International Pressure Ulcer Prevalence Survey," *Advances in Skin & Wound Care* 31, no. 6 (2018): 276–285, https://doi.org/10.1097/01.asw.0000532475.11971.aa.

8. C. Argoff, "Mechanisms of Pain Transmission and Pharmacologic Management," *Current Medical Research and Opinion* 27, no. 10 (2011): 2019–2031, https://doi.org/10.1185/03007995.2011.614934.

9. M. O. Urban and G. F. Gebhart, "Central Mechanisms in Pain," *Medical Clinics of North America* 83.3, no. 3 (1999): 585–596, https://doi.org/10.1016/s0025-7125(05)70125-5.

10. P. Rainville, "Brain Mechanisms of Pain Affect and Pain Modulation," *Current Opinion in Neurobiology* 12, no. 2 (2002): 195–204, https://doi.org/10.1016/s0959-4388(02)00313-6.

11. A. I. Basbaum and H. L. Fields, "Endogenous Pain Control Mechanisms: Review and Hypothesis," *Annals of Neurology: Official Journal*

of the American Neurological Association and the Child Neurology Society 4, no. 5 (1978): 451–462, https://doi.org/10.1002/ana.410040511.

12. C. J. Woolf, "Central Sensitization: Implications for the Diagnosis and Treatment of Pain," *Pain* 152.3, no. 3 (2011): S2–S15, https://doi.org/10.1016/j.pain.2010.09.030.

13. D. Vardeh, R. J. Mannion, and C. J. Woolf, "Toward a Mechanism-Based Approach to Pain Diagnosis," *Journal of Pain* 17, no. 9 (2016): T50–T69, https://doi.org/10.1016/j.jpain.2016.03.001.

14. N. B. Finnerup, R. Kuner, and T. Staehelin Jensen, "Neuropathic Pain: From Mechanisms to Treatment," *Physiological Reviews* (2020).

15. H.-G. Schaible and F. Richter, "Pathophysiology of Pain," *Langenbeck's Archives of Surgery* 389, no. 4 (2004): 237–243, https://doi.org/10.1007/s00423-004-0468-9.

16. S.-In Choi and W. H. Sun, "Depolarizing Effectors of Bradykinin Signaling in Nociceptor Excitation in Pain Perception," *Biomolecules & Therapeutics* 26, no. 3 (2018): 255–267, https://doi.org/10.4062/biomolther.2017.127.

17. E. E. Benarroch, "Ion Channels in Nociceptors: Recent Developments," *Neurology* 84, no. 11 (2015): 1153–1164, https://doi.org/10.1212/wnl.0000000000001382.

18. R. B. Stein, "Some Models of Neuronal Variability," *Biophysical Journal* 7, no. 1 (1967): 37–68, https://doi.org/10.1016/s0006-3495(67)86574-3.

19. A. L. Hodgkin and A. F. Huxley, "A Quantitative Description of Membrane Current and Its Application to Conduction and Excitation in Nerve," *Journal of Physiology* 117, no. 4 (1952): 500–544, https://doi.org/10.1113/jphysiol.1952.sp004764.

20. E. M. Izhikevich, "Simple Model of Spiking Neurons," *IEEE Transactions on Neural Networks* 14, no. 6 (November 2003): 1569–1572, https://doi.org/10.1109/tnn.2003.820440.

21. E. Dowlati, "Spinal Cord Anatomy, Pain, and Spinal Cord Stimulation Mechanisms," *Seminars in Spine Surgery* 29, no. 3 (2017): 136–146. WB Saunders, https://doi.org/10.1053/j.semss.2017.05.002.

22. R. Melzack and P. D. Wall, "Pain Mechanisms: A New Theory: A Gate Control System Modulates Sensory Input From the Skin Before It Evokes Pain Perception and Response," *Science* 150, no. 3699 (1965): 971–979, https://doi.org/10.1126/science.150.3699.971.

23. J. Braz, C. Solorzano, X. Wang, and A. I. Basbaum, "Transmitting Pain and Itch Messages: A Contemporary View of the Spinal Cord Circuits That Generate Gate Control," *Neuron* 82, no. 3 (2014): 522–536, https://doi.org/10.1016/j.neuron.2014.01.018.

24. Bo. Hjorth, "EEG Analysis Based on Time Domain Properties," *Electroencephalography and Clinical Neurophysiology* 29, no. 3 (1970): 306–310, https://doi.org/10.1016/0013-4694(70)90143-4.

25. C. S. Herrmann, D. Strüber, R. F. Helfrich, and A. K. Engel, "EEG Oscillations: From Correlation to Causality," *International Journal of Psychophysiology* 103 (2016): 12–21, https://doi.org/10.1016/j.ijpsycho.2015.02.003.

26. M. Siegel, T. H. Donner, and A. K. Engel, "Spectral Fingerprints of Large-Scale Neuronal Interactions," *Nature Reviews Neuroscience* 13, no. 2 (2012): 121–134, https://doi.org/10.1038/nrn3137.

27. C. S. Herrmann, M. Grigutsch, and N. A. Busch, "11 EEG Oscillations and Wavelet Analysis," in *Event-Related Potentials: A Methods Handbook*, Vol. 229, 2005).

28. R. Khazipov, M. Minlebaev, and G. Valeeva, "Early Gamma Oscillations," *Neuroscience* 250 (2013): 240–252, https://doi.org/10.1016/j.neuroscience.2013.07.019.

29. E. S. May, M. M. Nickel, S. Ta Dinh, et al., "Prefrontal Gamma Oscillations Reflect Ongoing Pain Intensity in Chronic Back Pain Patients," *Human Brain Mapp* 40.1, no. 1 (2019): 293–305, https://doi.org/10.1002/hbm.24373.

30. A. Williamson and B. Hoggart, "Pain: A Review of Three Commonly Used Pain Rating Scales," *Journal of Clinical Nursing* 14, no. 7 (2005): 798–804, https://doi.org/10.1111/j.1365-2702.2005.01121.x.

31. D. Ji, Y. Shi, J. Chen, Z. Zhao, and G. Zhao, "Mathematical Model for Skin Pain Sensation Under Local Distributed Mechanical Compression for Electronic Skin Applications," *Micromachines* 13, no. 9 (2022): 1402, https://doi.org/10.3390/mi13091402.